Astronomical and Astrophysical Transactions (*AApTr*), 2019, Vol. 31, Issue 2, pp. 75–88,
ISSN 1055-6796, Photocopying permitted by license only, ©Cambridge Scientific Publishers

Time variations of the total unsigned magnetic flux of active regions during the solar cycle 24

A.V. Zhukova*, V.I. Abramenko, A.S. Kutsenko

Crimean Astrophysical Observatory, Russian Academy of Sciences, Nauchny, Bakhchisaray, 298409, Crimea, Russia

Received 1 October, 2018

Ingredients of the total unsigned flux from all active regions (ARs) on the solar disc during cycle 24 (July 2010 to December 2017) were explored using line-of-sight magnetograms acquired by the Helioseismic and Magnetic Imager (HMI) onboard the Solar Dynamics Observatory (SDO). We classified ARs into three categories: A-type, regular bipolar ARs (attributed to global mean field dynamo); U-type, unipolar spots; B-type, irregular ARs, violating either Hale polarity law or Joy's law or having the leading spot less than the main following spot. A special subset of anti-Hale ARs (the most plausible result of small-scale turbulent dynamo) was formed by combining the subsets of anti-Hale ARs from both B and U categories. Total unsigned magnetic flux was calculated for each AR. In total, 1567 ARs with flux above 10^{20} Mx were detected.

Our inferences are:

i) One-rotation-averaged flux data show high cycle dependence for the A-type ARs (correlation coefficient $r = 0.84$) and very low cycle dependence for the anti-Hale ARs ($r = 0.36$).

ii) Depending on the cycle phase, 45–70% of the total flux comes from regular A-type ARs, 20–45% from irregular B-type ARs, 10–25% from unipolar spots. Anti-Hale ARs contribute up to 10% on occasional times during the maximum and their very low contribution grows from 3 to 6% as the minimum proceeds. Thus, during the maximum, the cycle-dependent fluctuations b of the mean field B contributes noticeably to the anti-Hale ARs production, along with the cycle-independent fluctuations h associated with small-scale dynamo.

iii) The amount of anti-Hale flux observed on an instant full-disc magnetogram in 2016–2017 (near minimum) is nearly constant on the level about 10^{21} Mx, which can be considered as the lower boundary of the small-scale dynamo productivity on spatial scales of ARs.

We can conclude that small-scale turbulent dynamo on scales of typical ARs displays a very weak productivity, which is approximately 2 orders of magnitude lower than disc-integrated unsigned flux from quiet-sun. However, the more important inference is that the small-scale turbulent dynamo is present deep in the solar interior (where ARs are rooted) and is not restricted by the near-surface layer of the convective zone.

Keywords: Sun: magnetic fields – Sun: photosphere – Sun: sunspots – Sun: activity

*Email: anastasiya.v.zhukova@gmail.com

1 Introduction

The global solar magnetic field is believed to be produced by the traditional mean-field dynamo mechanism (Moffat 1978; Krause and Radler 1980), see also reviews by Ossendrijver (2003), Brandenburg and Subramanian (2005), Brandenburg et al. (2012), Charbonneau (2014). However, the variety of small-scale mixed-polarity magnetic elements visible in the quiet-Sun (QS) photosphere can hardly be explained by the mean-field dynamo (however, see Stenflo and Kosovichev (2012), where the authors argue that the small-scale fields can be a result of the turbulent cascade, i.e., fragmentation of the global magnetic structures generated by the mean-field dynamo). As it follows from the dynamo theory (see, e.g., reviews by Brandenburg et al. (2012) and Sokoloff et al. (2015)), the dynamo-generated field consists of three parts: the cycle-dependent mean field B, fluctuations b produced by fragmentation of B (which are also cycle-dependent), and, finally, the cycle-independent fluctuations h, which are produced independently of B by small-scale turbulent dynamo. Generally speaking, excitation of the h-type fluctuations can occur not only on smallest observable scales as it follows from MHD-simulations (Cattaneo 1999; Vogler and Schussler 2007; Pietarila Graham et al. 2010; Karak and Brandenburg 2016), but also on scales of a typical AR, see, e.g., Sokoloff et al. (2015). The authors suggested diagnostics of small-scale turbulent dynamo based on statistical analysis of sunspot groups which violate the Hale polarity law (Hale et al. 1919; Hale and Nicholson 1925).The prevalence of Hale polarity law and the Joy's law for magnetic bipoles are essential conditions for Babcock-Leighton model of polar-field reversal (Babcock 1961; Leighton 1964) and, therefore, for the mean-field dynamo models, see e.g. Schrijver and Zwaan (2000). The Hale polarity law states that during an even (odd) sunspot cycle, leading sunspots in the northern hemisphere have negative (positive) polarity and it is opposite to that in the southern hemisphere. In cases when this rule is not met, the sunspot group is classified as anti-Hale AR. The Joy's law describes the tilt of magnetic bipoles relative to the east-west direction. The leading (westward) spot is usually located closer to the equator than the following spot, and the average tilt becomes steeper with increasing latitude (Hale et al. 1919). Following Wang and Sheeley (1989), one can accept that the Joy's law is met when absolute value of the tilt (an angle between the equator and AR axis connecting the leading and following parts of the AR) does not exceed 20 degrees and the leading spot is closer to the equator than the following spot(s).

These laws were explored intensively using a variety of available solar data (Wang and Sheeley 1989; Li and Ulrich 2012; Stenflo and Kosovichev 2012; McClintock et al. 2014; Illarionov et al. 2015; Sokoloff et al. 2015, to mention a few).

In addition, the third "pillar" of the mean-field dynamo theory is a prevalence of the leading spot: leading sunspots are found to be usually larger and more coherent than the following ones, see, e.g., a review by van Driel-Gesztelyi and Green (2015). Babcock (1961) in his phenomenological dynamo model paid special attention to the "preponderance" of leading spots: "Preceding spots of a group tend to be larger and to have a longer lifetime than f spots (Grotrian and Kunzel 1950). The mean ratio of the effective flux in the spots is about 3:1". Babcock explained this as an influence of the Coriolis force on an emerging Ω-loop in full agreement with his model.

Deviations from the above-mentioned laws can be considered as manifestation of participation of local turbulent dynamo in the convective zone, as the flux tube

emerges. Anti-Hale sunspot groups are thought to be the most plausible results of the small-scale turbulent dynamo action on scales of typical ARs (see, e.g., Stenflo and Kosovichev (2012); Sokoloff et al. (2015)). Sokoloff et al. (2015) found that the ratio of the number of anti-Hale ARs to the total number of ARs attains the maximal value during the period of the solar minimum. Taking into account that the total number of ARs is very low during the minimum, one must conclude that the enhanced aforementioned ratio implies that the number of the anti-Hale groups does not depend on the cycle, or, in other words, the effect can be treated as a support for the small-scale dynamo action in the convection zone on the spatial scales of ARs. It is worth noting, however, that not all anti-Hale ARs have to be attributed to small-scale turbulent dynamo, i.e., h-fluctuations. A part of them can be a result of mean-field dynamo fluctuations, b (Sokoloff et al. 2015). Therefore, the best epoch to test the small-scale dynamo productivity would be periods of solar minima, when mean field B and its fluctuations b are lowest.

A comprehensive analysis of ARs average properties over a solar cycle was performed for the first time by Wang and Sheeley (1989) using 2700 bipolar magnetic regions of the 21st solar cycle (the strongest of the recent five cycles). Their magnetic fluxes were derived using empirical rules from full-disk magnetograms and photographic images taken at the National Solar Observatory Kitt Peak. The authors reported that only 4% of ARs violated Hale polarity rule and the average AR magnetic flux decreased as the cycle progressed from $(5–6)\times10^{21}$ Mx in 1977 to 3×10^{21} Mx in 1985. At the same time, the averaged magnetic flux of anti-Hale and non-Joy ARs demonstrated a slight enhancement during the solar minimum (1984–1986).

We make an attempt to extend previous researches by using space-born solar data and focusing on the weakest cycle out of the recent five ones. SDO data set also gives us a possibility to analyse not only the number of ARs, but also to take into account the magnetic flux of ARs. Our aim was to estimate contributions into the total unsigned flux from ARs of different types (described in Section 2.2) and to track the partial flux variations through the cycle. We expect that a gradual transition from statistical properties of the mean-field-dynamo-generated regular ARs toward the anti-Hale ARs can help us to reveal the interplay between the mean-field dynamo and small-scale turbulent dynamo contributions.

2 Data and method

2.1 Data processing

Magnetographic data acquired by the Helioseismic and Magnetic Imager (HMI), see Scherrer et al. (2012), onboard the Solar Dynamic Observatory were utilized. The magnetograms were taken in the FeI 6173.3 Å spectral line with the spatial resolution of 1″ and pixel size of 0.5″ (Schou et al. 2012; Liu et al. 2012). Space-weather HMI Active Region Patches (SHARPs) sharp_cea_720s data, namely, line-of-sight (LOS) magnetograms and continuum images (Bobra et al. 2014) were used. To verify magnetic connections within ARs, we also used the Fe IX/X 171 Å and 193 Å data obtained with the SDO/AIA instrument (Lemen et al. 2012). Note that sharp_cea_720s data provide the LOS component of the magnetic field remapped on the grid corrected for the projection effect (Bobra et al. 2014).

The 8-year long magnetographic data set (from 2010 June 7 to 2017 December 31) covering the rise, maximum and descending phases of the 24th solar cycle, were offered by SDO mission. It allows us to study changes of particular physical quantities with a cycle. Moreover, SDO data made possible a more detailed classification of ARs.

Our purpose is to reveal a composition of the total magnetic flux, namely, to estimate what part of the flux is linked to the global mean field dynamo and what fraction might be attributed to influence of the local turbulent dynamo. A common approach for such purposes is to analyse independent instant images of the process under study. The easiest way would be to take one image of the sun per, say, a half-year interval. However, statistics would be very low. Another way is to take a full-disc image every half-rotation. In this case, near-limb ARs would be counted with very low quality. We selected to take three evenly-spaced images per rotation, each covering the central part of the disc. Thus, every 9th day starting 2010 June 7 was selected for study. Strictly speaking, we then have to restrict ourselves with the longitudinal interval from –60 to +60 degrees (three 120-degree intervals cover the whole round) to form a sequence of non-overlapping images. However, with the aim to increase statistics (especially during the most interesting times near minima), we selected ARs in the (–70, +70) degree longitudinal interval. We then dropped the second entry for ARs which observed near both limbs, leaving the closest to the disc center one. We acknowledge that the proposed routine has certain shortcomings. First, a part of ARs (about 6%, according to Waldmeier (1950, Ch. 6) and Gnevyshev (1938)) survive longer than one rotation, so that 9-day-separated images cannot be always independent. Second, our routine can miss some short-lived ARs (less than 9 days) formed near the eastern limb. To mitigate the latter, one should repeat the routine 9 times with a one-day shift of the starting data and then to average the results, which is our future plans.

In each case, the magnetogram obtained at 05:24:00 UT was selected. At this specific time, influence of the artificial 24-hour oscillations of the HMI magnetic flux is close to zero (Kutsenko, Abramenko 2016).

It was impossible to consider SHARP magnetograms as individual cases for the study because frequently a patch encloses more than one AR. In such cases, the patch was divided, and each AR was listed separately under its NOAA number. The magnetograms were cropped to enclose the main features of the AR and to minimize the surrounding area of quiet sun.

The total unsigned magnetic flux of an AR was retrieved from the radial component of the magnetic field, $B_{\rm R}$, obtained from $B_{\rm LOS}$ by dividing over the cosine of the angle μ, the angle between the normal to the solar surface and the LOS direction (Hagenaar 2001). Then, the summing of absolute values of the magnetic field strength was performed over all pixels exceeding the double standard deviation noise level of 12 Mx cm^{-2} (Liu et al. 2012). We considered only ARs with total unsigned flux exceeding 10^{20} Mx. In total, we selected 1567 ARs.

2.2 Classification of ARs

The three aforementioned criteria for mean-field global dynamo were accepted for classification of ARs. Visual inspection of the morphology of sunspots, evolution, magnetic connections, and other evolutionary properties, allowed us to assign each

AR in our list to one of the following categories:

(A) ARs that satisfy the mean-field dynamo requirements: a bipolar AR obeying Hale polarity law, Joy's law and having the leading spot larger than the main following spot (regular ARs);

(U) unipolar sunspots (compact single spots without any pores/spots around that can be considered as the remains of the following part);

(B) all the rest (irregular) ARs. This category includes violators of Hale and/or Joy's laws, or ARs with leading spot smaller than the main following spot.

(Anti-Hale) a special subset formed combining anti-Hale ARs from both B and U categories.

The hierarchy of the categories is presented schematically in Fig. 1, and the parameters are listed in Table 1.

The criterion of Joy's law fulfilment requires careful analysis, especially in two cases. First, when analysing emerging ARs, because the tilt can vary notably during first several days following the beginning of the AR emergence (van Driel-Gesztelyi and Green 2015). In such cases, we followed the development of an AR until a stable tilt was achieved and this tilt angle was used in the study. Second, when the following sunspots formed a fan-like structure of scattered pores/spots, the tilt was defined as a bisector between two lateral lines enclosing the following part and intersecting the center of the leading sunspot. We accept that Joy's law is met when the absolute value of the tilt angle does not exceed 20 degrees (Wang and Sheeley 1989) and the leader is closer to equator than the following part. Note that for all ARs, judgement about the Joy's law fulfilment was made on the basis of continuum images of the sunspot groups.

The criterion about a relationship between leading and following sunspots requires additional clarification. During emergence the leading part displays a tendency to be

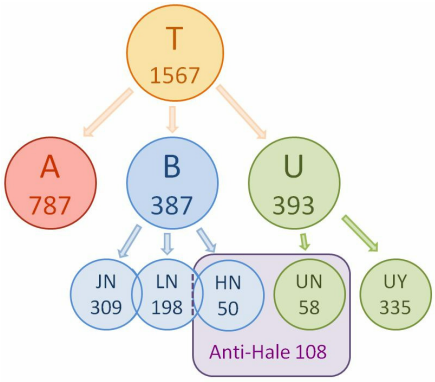


Figure 1 Hierarchy of AR categories and the number of detected events: T – total number of ARs, A – regular bipolar AR obeying Hale and Joy's laws and having the leading sunspot larger than the main following sunspot; B – irregular bipolar or multi-polar ARs (violating at least one of the aforementioned laws); U – unipolar spots; JN – ARs violating the Joy's law; LN – ARs with the main following spot larger than the leading spot; HN – anti-Hale bipolar or multi-polar ARs; UN – unipolar anti-Hale spots; UY – regular polarity unipolar spots. The subset of all anti-Hale ARs is enclosed by a rectangle.

Table 1 Types of ARs and statistical parameters.

	All ARs, T	Type A	Type B	All anti-Hale, HN+UN	Uni-polar, U	Unipolar Hale, UY	Unipolar anti-Hale, UN
Number of ARs	1567	787	387	108	393	335	58
Number of rot.	103	103	89	59	98	97	40
Correlation with total flux	1.0	0.84	0.72	0.36	0.51	0.48	0.16
95% confidence interval		0.77–0.89	0.60–0.81	0.11–0.56	0.35–0.64	0.31–0.62	–0.16–0.45

advected into a compact pore/spot whereas the following part stays more fragmented (e.g., Lites et al. 1998, van Driel-Gesztelyi and Green 2015), so that the leading spot is usually larger than any following spots. Also, the leading spot usually emerges faster and lasts longer (see, for example, a review by van Driel-Gesztelyi and Green (2015) and a recent work by Norton et al. (2017)). We used this criterion, and those ARs with the area of the leading sunspot smaller than that of the dominant following sunspot were not included in the type A category.

The majority of unipolar spots are the remains of a strongest spot of an AR, predominantly, of leading spot. Then the Hale-law test can be applied for them. This gave us a possibility to divide ARs of U-type category into two subsets: unipolar sunspots (UY, Unipolar Yes) that obey the Hale polarity law, and anti-Hale unipolar spots, (UN, Unipolar No). When classifying a spot as a UN-type, we made sure that a spot is a remnant of a leading part of an AR (in accordance with the definition of anti-Hale group), using AIA images of the coronal magnetic loops structure and the evolution history.

The set of B-type ARs was split into three overlapping subsets: bipolar ARs with wrong tilt, JN (JN, Joy No); bipolar/multi-polar ARs, which violate the Hale polarity law, HN (Hale No); and finally, bipolar ARs with the area of the main following spot exceeding the area of the leading spot, LN (Leader No). Note that an irregular AR (especially very complex ones) can belong to several subsets, for example, an AR with wrong tilt might have a dominant sunspot located in the following part. That is why the subsets JN, HN, LN are overlapping. (Results of the statistical analysis of these subsets will be a subject of our future publications, and here we mention them to clarify the classification routine.)

Special attention was given to a subset of all detected anti-Hale groups, i.e., a combined subset of HN and UN types. We will refer to this subset as "all anti-Hale" ARs and their combined magnetic flux as "all-anti-Hale flux" (see the 5th column of Table 1). Figure 2 shows the latitude-time diagram (butterfly diagram) for them. We see that our statistics are not contaminated by new high-latitude ARs belonging to the next solar cycle 25. Later, during the solar minimum this contamination will become significant and pose a serious problem, see, e.g., McClintock et al. (2014) and Sokoloff (2015).

More details of ARs selection routine, as well as the list of the total flux for each AR, can be found in Zhukova (2018).

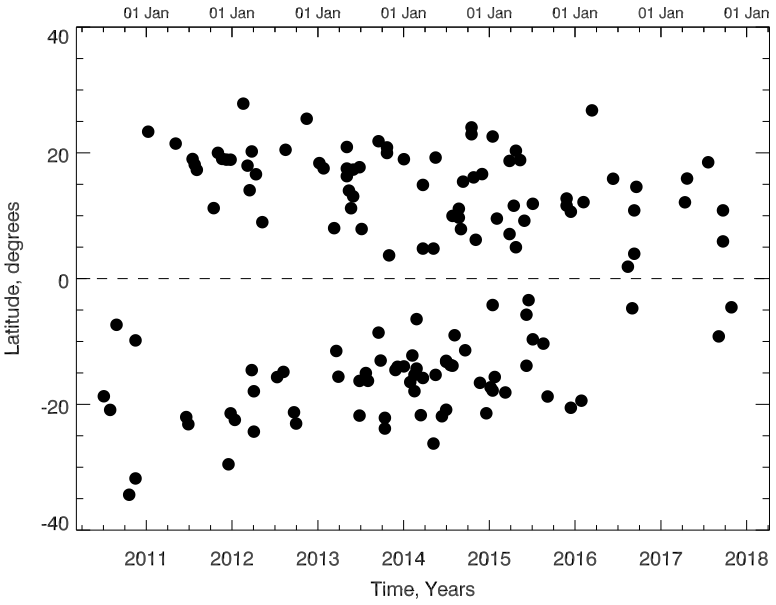


Figure 2 Butterfly diagram of all anti-Hale ARs.

3 Results

Having the unsigned magnetic flux calculated for each AR for a given day and summing flux over all ARs for a given day, we obtain total unsigned flux per day, T, from all ARs over the visible solar surface (of cause, within 70° distance from the disk center). For 309 observation days (according to the number of 9-day intervals from the beginning to the end of our period of investigation), this flux is plotted with black circles in Fig. 3. We also plot there the similarly calculated total flux per day contributed by A-type (blue circles) and B-type ARs (red circles). The data points are very crowded and give only a general impression of matching the cycle variations.

To explore whether the obtained flux T reflects the cycle variations of the solar magnetic field, we attempt a comparison with the sunspot areas provided by the Royal Observatory, Greenwich – USAF/NOAA Sunspot Data, https://solarscience.msfc.nasa.gov/greenwch.shtml. In Fig. 4 we overplot the rotation-averaged flux T with the rotation-averaged sunspot area. The former was computed by averaging T_i over three observation days (which cover a 27-day period); the latter was found by averaging over the same 27 days from the USAF-data list. The overlapping data points were used to derive the Pearson correlation coefficient, which was found to be 0.86 with the 95% confidence interval of 0.77–0.89. The obtained accordance between the estimated flux T and the sunspot areas data suggests that cycle-related variations of solar magnetic activity are well reflected by the obtained data set T. Below we will use the data set T to judge the cycle dependence of other parameters.

The routine described above, of flux averaging over rotation was applied to all categories. The corresponding Pearson correlation coefficients, as well as 95% confidence intervals are gathered in the 3rd and 4th rows of Table 1. We see that the

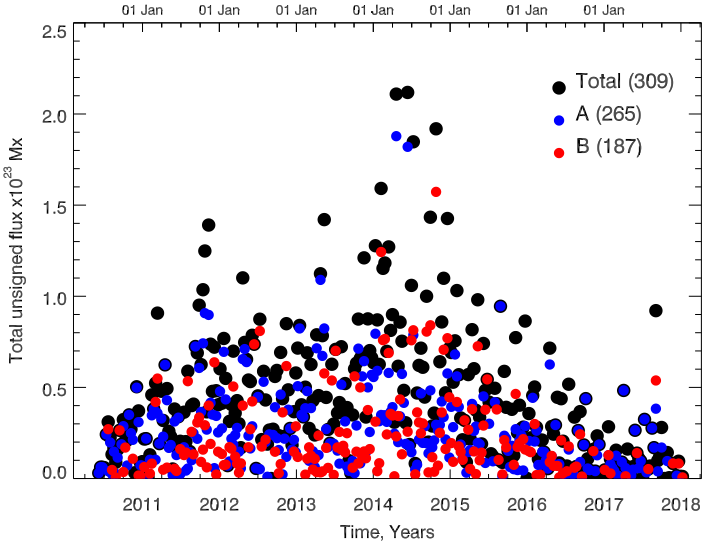


Figure 3 The unsigned flux per day from all ARs of a given category on the disk. The number of observation days is shown in parentheses.

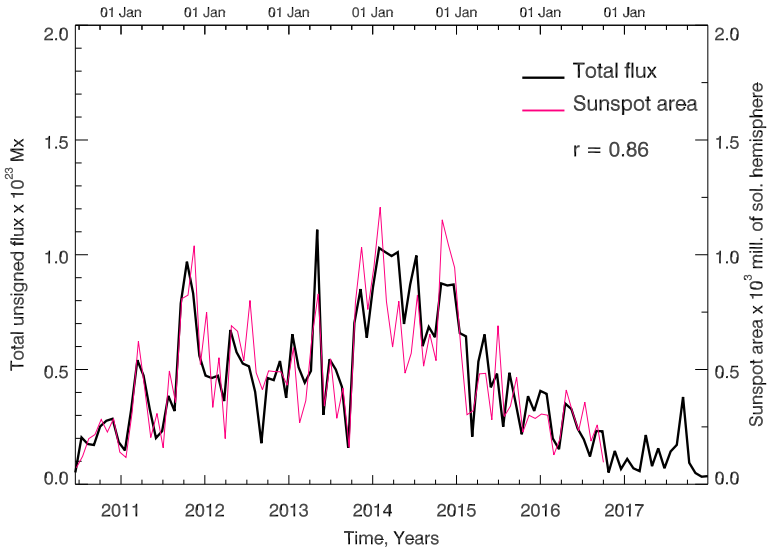


Figure 4 Averaged over rotation total flux, T, from all detected ARs (thick black curve) and the same way averaged sunspot areas, thin magenta curve. The Pearson correlation coefficient, r, is shown.

ensemble of A-type ARs shows the highest correlation with T, $r = 0.84$. This is in accordance with a notion that regular ARs (obeying Hale and Joy's laws and revealing prevalence on the leading spot – the essential mean field dynamo requirements) are the most plausible candidates to be generated by mean-field dynamo and to follow

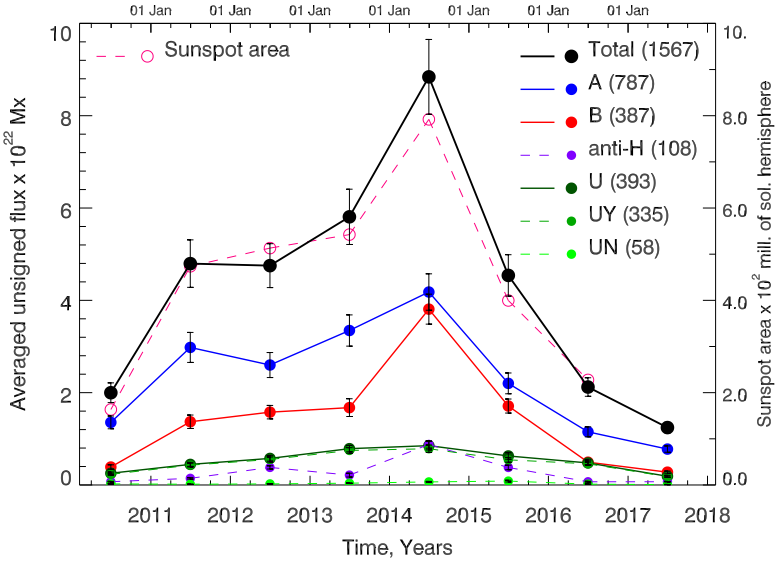


Figure 5 Yearly-averaged flux from (all on the disk) ARs of a given category. Magenta dashed curve shows the sunspot areas. The number of events (ARs) is shown in parentheses.

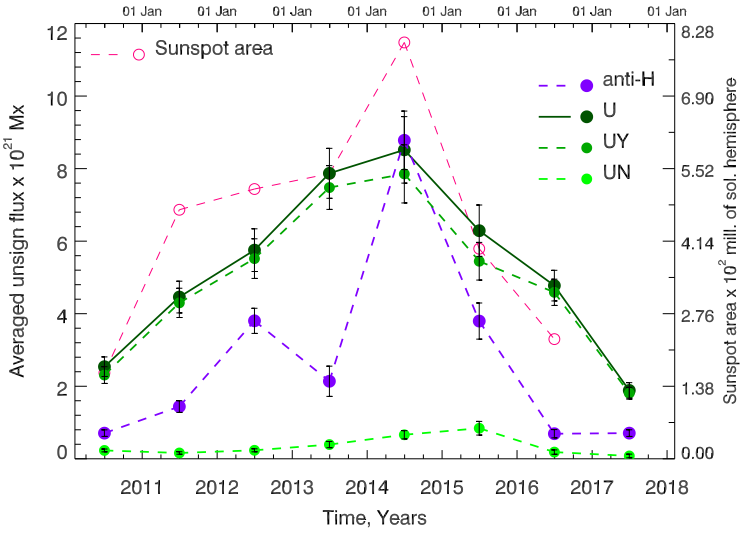


Figure 6 The same as in Fig. 5 but the vertical axis is extended.

the solar cycle. Interestingly, the B-type ARs show only a slightly lower correlation with T than the A-type ARs do. We find low correlation ($r = 0.36$) for the ensemble of all anti-Hale groups (5th column in Table 1). Unipolar spots U and especially the anti-Hale unipolar subset, demonstrate rather low correlation with the total flux.

To reveal flux changes with the solar cycle, we performed the one-year averaging of the flux per day for different types of ARs. Results are shown in Figs 5 and 6.

(Note the difference in the vertical axis scale in the figures.) Observational errors of the flux were derived based on the 3-sigma noise level of SDO/LOS data, which is 18 Mx×cm^{-2} and includes all possible uncertainties of magnetic field density acquisition, according to Liu et al. (2012). Flux uncertainties in pixels were summed over a magnetogram. Then errors of flux calculation for each magnetogram were summed over all corresponding ARs on the disc for each observation day and the sums were averaged over a year (i.e., over 39–40 observation days). The plots demonstrate that the dominant contribution to the total flux, T, comes from the A-type ARs (blue circles). A bit lower but quite comparable contribution comes from all irregular, B-type ARs. Unipolar spots (green circles and solid green line) provide the lowest addition to the total flux with a slight overall correspondence to the cycle.

Anti-Hale groups deserve a special attention. In 2016–2017 (beginning of the oncoming minimum), all but anti-Hale fluxes decreased in accordance to the cycle, whereas the yearly-averaged flux from all anti-Hale groups stayed unchanged in 2016 and 2017 (see Fig. 6). Moreover, at the end of the previous solar minimum (in 2010) the anti-Hale flux during that time achieved the same level of about 7.1×10^{20} Mx. During solar maximum, the flux from all anti-Hale groups was elevated and it reached 9×10^{21} Mx level in 2014. Note that for unipolar anti-Hale spots the enhancement in the maximum is less pronounced (compare the purple and light green dashed lines in Fig. 6).

To reveal the relative contributions from ARs of different types into the total flux, we calculated the ratio of the yearly-averaged fluxes to the total yearly-averaged flux, T, for each type of ARs (Fig. 7). The greatest contribution (from 45 to 70%) always comes from the A-type (regular) ARs, while 20% to 45% of flux comes from B-type (all irregular) ARs, and the rest is contributed by unipolar spots. The observed large scattering of ratios is related to the cycle dependence of contributions, as it

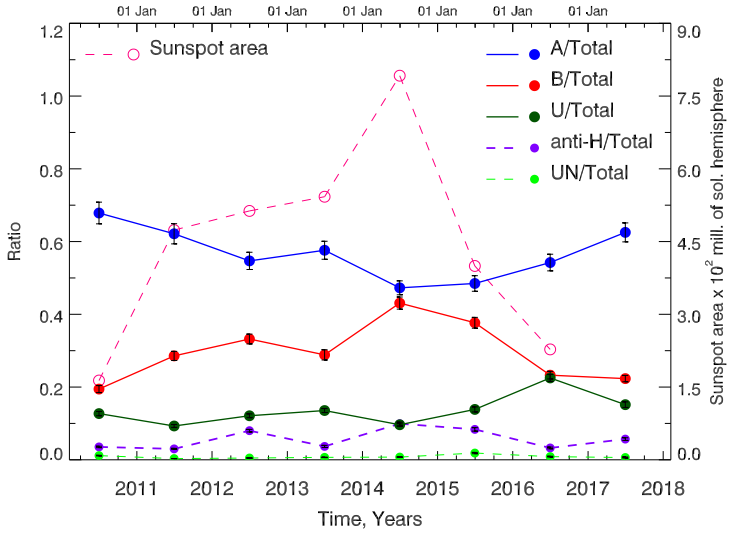


Figure 7 Yearly-averaged ratios of the total flux in each category to the total flux T from all ARs. Notations are the same as in Fig. 5.

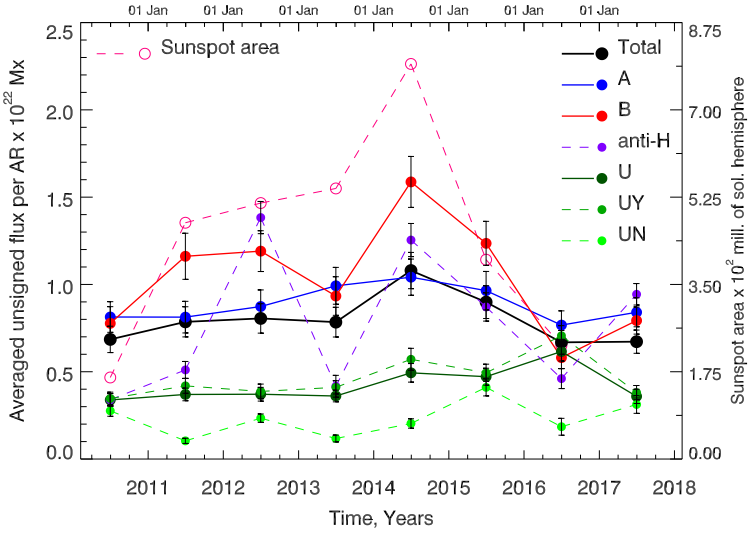


Figure 8 Yearly-averaged values of the averaged (per AR) flux for a given category. Notations are the same as in Fig. 5.

follows from trends in Fig. 7. Indeed, as the cycle progresses to its maximum, from 2010 to 2014, the fraction of flux from the A-type ARs monotonously decreases whereas that of the irregular ARs increases. The opposite tendency is noticeable during the descending phase. The phenomenon might be explained by reinforcement of fluctuation part, b, of the mean field during the cycle maximum.

All anti-Hale ARs contribute up to 10% of the total flux during the solar maximum with the average (over 8 years) value of about 6%. As the oncoming minimum overtakes (2016–2017), the fraction of the anti-Hale flux increases from 3% to 6%, see Fig. 7.

As for statistical properties of ARs of a given type, our database allows us to derive the average flux per AR for each type of ARs. When calculating the average flux per AR for a given category, the summed over year flux from all ARs (of a given category) was divided over the number of such ARs. The results are presented in Fig. 8. A smooth maximum near 2014-2015 reaching 1.0×10^{22} Mx is observed for the A-type ARs, which are not the strongest type in this cycle. At the same time, B-type ARs demonstrate abrupt time variations and the strongest flux per AR, up to 1.6×10^{22} Mx with the two peaks roughly coinciding with the sunspot-area maxima. The time profile for all anti-Hale ARs nearly follows the B-type ARs profile, also showing abrupt changes. Note that toward the solar minimum (2016–2017), the irregular and anti-Hale groups became stronger. Unipolar spots are weakest ARs in our study, the flux per AR slightly varies with cycle, and only UN demonstrate a hint of accordance with the cycle peaks.

Concluding remarks

Uniform, space-born magnetic field data from SDO/HMI instrument obtained during 2010–2017 allowed us to study the statistical behaviour of the magnetic flux in ARs during rising, maximum and descending phases of the 24th solar cycle. We classified ARs into several categories/groups: A-type ARs (regular bipolar ARs); U-type ARs – unipolar spots; B-type ARs – irregular ARs, violating either Hale polarity law, or Joy's law, or having the following main spot larger than the leading spot. A subset of all anti-Hale ARs was created by combining anti-Hale ARs from both B and U categories. Total unsigned flux, T, determined for all ARs observed on the visible solar disk was explored, and special attention was paid to contributions from the aforementioned categories of ARs. The following conclusions were formulated.

1. Magnetic flux of A-type ARs makes the greatest contribution to the total flux T. This result is in agreement with the well-known concept that the mean-field dynamo mechanism plays the key role in generation of the organized toroidal flux system in the convection zone and the 11-year cyclicity of solar magnetic activity. However, the time profiles of the total flux and A-type-ARs flux are well apart indicating that not only the mean field, B, but also the fluctuating components, both b and h, reveal their footprints on the surface.

2. Connection with the solar cycle gradually decreases with transition from A-type to B-type to unipolar spots to anti-Hale ARs. The tendency is well pronounced in Pearson correlation coefficients for one-rotation-averaged data showing that their correlation with the total unsigned flux diminishes from 0.84 to 0.72 to 0.51 to 0.36, respectively. The data suggest that whereas the flux from regular ARs varies in accordance with cycle (and, therefore, might be attributed to mean-field dynamo), the flux from anti-Hale ARs practically is not correlated with cycle, and, therefore, at least, part of it, might be attributed to small-scale turbulent dynamo.

3. Contributions into the total flux by different AR categories varies in the following limits: 45–70% comes from regular A-type ARs, 20–45% from irregular B-type ARs, 10–25% from unipolar spots. We found no monotonous decrease of the flux ratio with the progress of the cycle, contrary to the findings reported by Wang and Sheeley (1989). Instead, during the rise phase we observe a gradual increase of the B-type ARs contribution simultaneously with diminishing contribution of the A-type ARs. After maximum, the opposite tendencies overtake.

4. The fraction of anti-Hale AR flux increases from 3 to 6% during 2016–2017, i.e., near the solar minimum. So, as the cycle strength ceases, anti-Hale flux tends to overtake becoming more pronounced on the background of very weak mean field B and its fluctuations b. However, during maximum, the fraction of anti-Hale ARS can reach sometimes up to 10%. This might be explained by reinforcement of b-fluctuations, which also can produce anti-Hale ARs (Sokoloff et al. 2015). We conclude that small-scale turbulent dynamo productivity can be estimated during periods of low solar activity.

5. The amount of anti-Hale flux observed on an instant full-disc magnetogram in 2016–2017 is about 10^{21} Mx, which can be considered as the lower boundary of the small-scale dynamo productivity on spatial scales of ARs.

6. Analysis of the flux-per-AR values shows that i) irregular ARs (B-type) demonstrate highest amount of flux per AR (up to 1.6×10^{22} Mx) whereas regular A-type

ARs exhibit lower fluxes in a range of (0.8–1.0)$\times 10^{22}$ Mx per AR with a smooth peak around the solar maximum. The anti-Hale flux per AR shows abrupt variations in a range of (0.3–1.4)$\times 10^{22}$ Mx with two peaks in 2012 and 2014, nearly synchronously with the solar activity maxima. This allows us to conclude that generation of anti-Hale groups during a solar maximum may be due to both the mean-field dynamo (via reinforcement of cycle-dependent fluctuations b) , and by the small-scale turbulent dynamo action, i.e., via h-fluctuations. So, during a solar maximum, it is hardly possible to separate actions of mean-field and small-scale dynamos on scales of ARs.

Our statistical study shows that small-scale turbulent dynamo on scales of typical ARs displays a very weak productivity, about 10^{21} Mx over disc, which is approximately 2 orders of magnitude lower than disc-integrated unsigned flux from quiet-sun (Jin et al. 2011). However, the more important point here is the fact that the small-scale turbulent dynamo is present deep in the solar interior (where ARs are rooted) and is not restricted by the near-surface layer of the convective zone.

Acknowledgements

We are grateful to anonymous Referee for fruitful comments and criticism, which helped much to improve the paper. SDO is a mission for NASA Living With a Star (LWS) program. The SDO/HMI data were provided by the Joint Science Operation Center (JSOC). The study was supported by the Russian Science Foundation (Project 18-12-00131).

References

Babcock, H.W., 1961, Astrophys. J., 133, 572
Bobra, M.G., Sun, X., Hoeksema, J.T., Turmon, M., Liu, Y., Hayashi, K., Barnes, G., Leka, K.D., 2014, Solar Phys., 289, 3549
Brandenburg, A., Subramanian, K., 2005, Phys. Reports, 417, 1
Brandenburg, A., Sokoloff, D., Subramanian, K., 2012, Space Science Rev., 169, 123
Cattaneo, F., 1999, Astrophys. J., 515, L39
Charbonneau, P., 2014, Ann. Rev. Astron. Astrophys., 52, 251
Gnevyshev, M.N., 1938, Pulkovo Observatory Circular, 24, 37
Grotrian, W., K*ü*nzel, H., 1950, Zeitschrift fuer Astrophysik, 28, 28
Hagenaar, H.J., 2001, Astrophys. J., 555, 448
Hale, G.E., Ellerman, F., Nicholson, S.B., Joy, A.H., 1919, Astrophys. J., 49, 153
Hale, G.E., Nicholson, S.B., 1925, Astrophys. J., 62, 210
Illarionov, E., Tlatov, A., Sokoloff, D., 2015, Solar Phys., 290, 351
Jin, C. L., Wang, J.X., Song, Q., Zhao, H., 2011, Astrophys. J., 731, 37
Karak, B.B., Brandenburg, A., 2016, Astrophys. J., 816, 28
Krause, F., R*ä*dler, K.H., 1980, Mean-Field Magnetohydrodynamics and Dynamo Theory (Akademie-Verlag, Berlin)
Kutsenko, A.S., Abramenko, V.I., 2016, Solar Phys., 291, 1613
Leighton, R.B., 1964, Astrophys. J., 140, 1547

Lemen, J.R., Title, A.M., Akin, D.J., Boerner, P.F., Chou, C. and 42 co-authors, 2012, Solar Phys., 275, 17
Li, J., Ulrich, R.K., 2012, Astrophys. J., 758, 115
Lites, B.W., Skumanich, A., Martínez, P., V., 1998, Astron. Astrophys., 333, 1053
Liu, Y., Hoeksema, J.T., Scherrer, P.H., Schou, J., Couvidat, S., Bush, R.I., Duvall, T.L., Hayashi, K., Sun, X., Zhao, X., 2012, Solar Phys., 279, 295
McClintock, B.H., Norton, A.A., Li, J., 2014, Astrophys. J., 797, 130
Moffat, H.K., 1978, Magnetic Field Generation in Electrically Conducting Fluids (Cambridge Univ. Press, Cambridge, U.K., New York, U.S.A.)
Norton, A.A., Jones, E.H., Linton, M.G., Leake, J.E., 2017, Astrophys. J., 842, 3
Ossendrijver, M., 2003, The Satron Astrophis. Rev., 11,287
Pietarila Graham, J., Cameron, R., Schüssler, M., 2010, Astrophys. J., 714, 1606
Scherrer, P.H., Schou, J., Bush, R.I., Kosovichev, A.G., Bogart, R.S., and 8 co-authors, 2012, Solar Phys., 275, 207
Schou, J., Scherrer, P. H., Bush, R. I., Wachter, R., Couvidat, S. and 16 co-authors, 2012, Solar Phys., 275, 229
Schrijver, C.J., Zwaan, C., 2000, Solar and Stellar Magnetic Activity (Cambridge, Cambridge Univ. Press)
Sokoloff, D., Khlystova, A., Abramenko, V., 2015, Monthly Notices of the Royal Astronomical Society, 451, 1522
Stenflo, J.O., Kosovichev, A.G., 2012, Astrophys. J., 745, 129
van Driel-Gesztelyi, L., Green, L.M., 2015, Liv. Rev. Solar Phys., 12, 1
Vögler, A., Schüssler, M., 2007, Astron. Astrophys., 465, L43
Waldmeier, M. 1950, Results and Problems of Investigation of the Sun, Foreign Literature Press, Moscow
Wang, Y.M., Sheeley, N.R. Jr., 1989, Solar Phys., 124, 81
Zhukova, A.V., 2018, Bull. Crimean Astrophys. Observ., 114, 74